Cell Reports, Volume *34*

Supplemental Information

Electron Microscopic Reconstruction of Neural Circuitry in the Cochlea

Yunfeng Hua, Xu Ding, Haoyu Wang, Fangfang Wang, Yan Lu, Jakob Neef, Yunge Gao, Tobias Moser, and Hao Wu

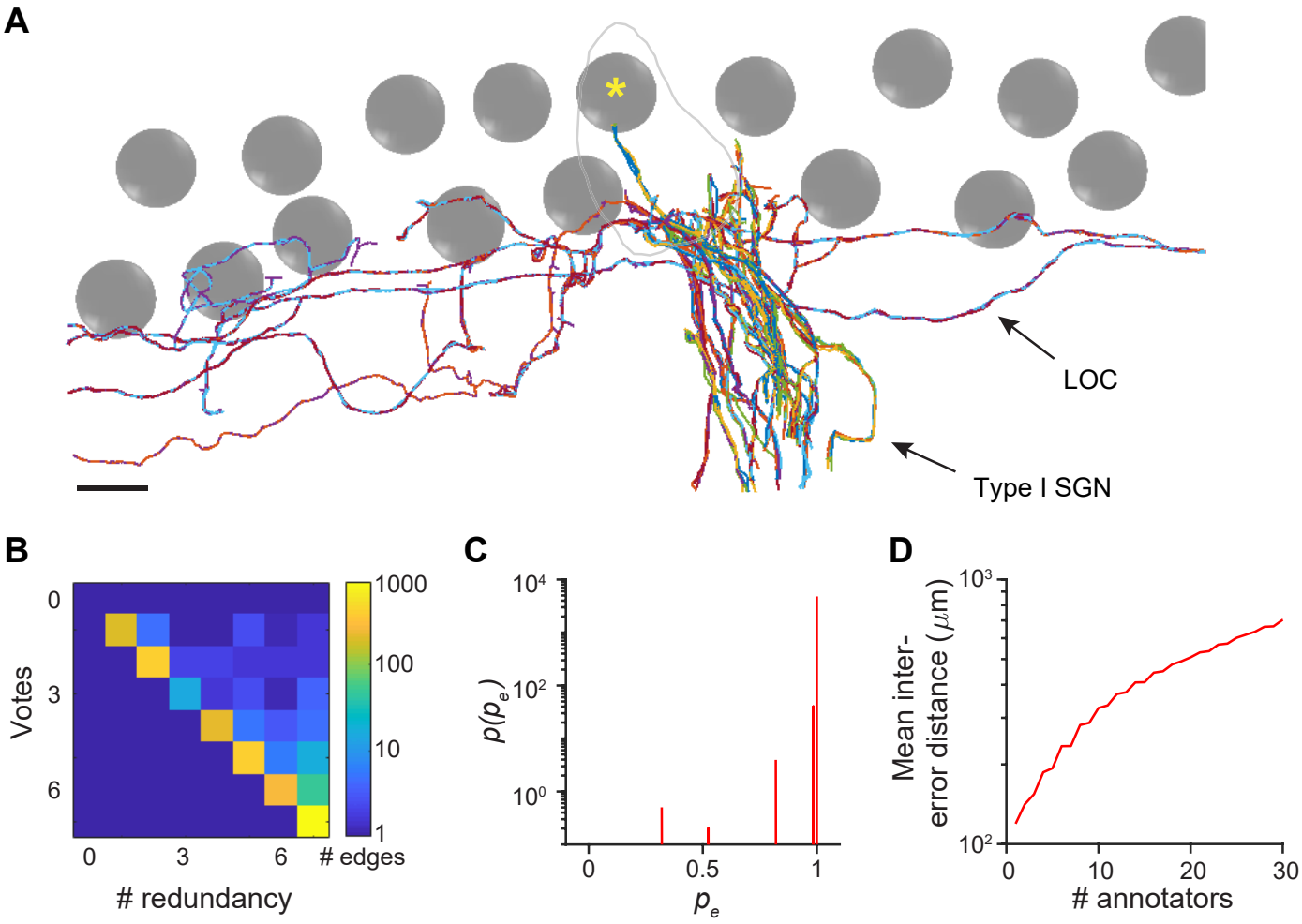

Figure S1. Quantification of tracing accuracy. Related to Figure 1 (A) 7-fold skeletonization of the type I SGN-dendrites and an efferent axon traced by trained non-experts in the dataset. For SGN-dendrites, all tracing started from the ribbon-type AZ and proceeded to the heminode of the SGN-dendrite. Grey spheres represented the nuclei of IHCs which were arranged in a staggered manner. Scale bar 5 µm. (B-D) RESCOP analysis of traceability: histogram of edge votes (B), estimated edge-detection probability $p(p_e)$ distribution for all traced neurites (C), and prediction of tracing accuracy as a function of annotation redundancy (D).

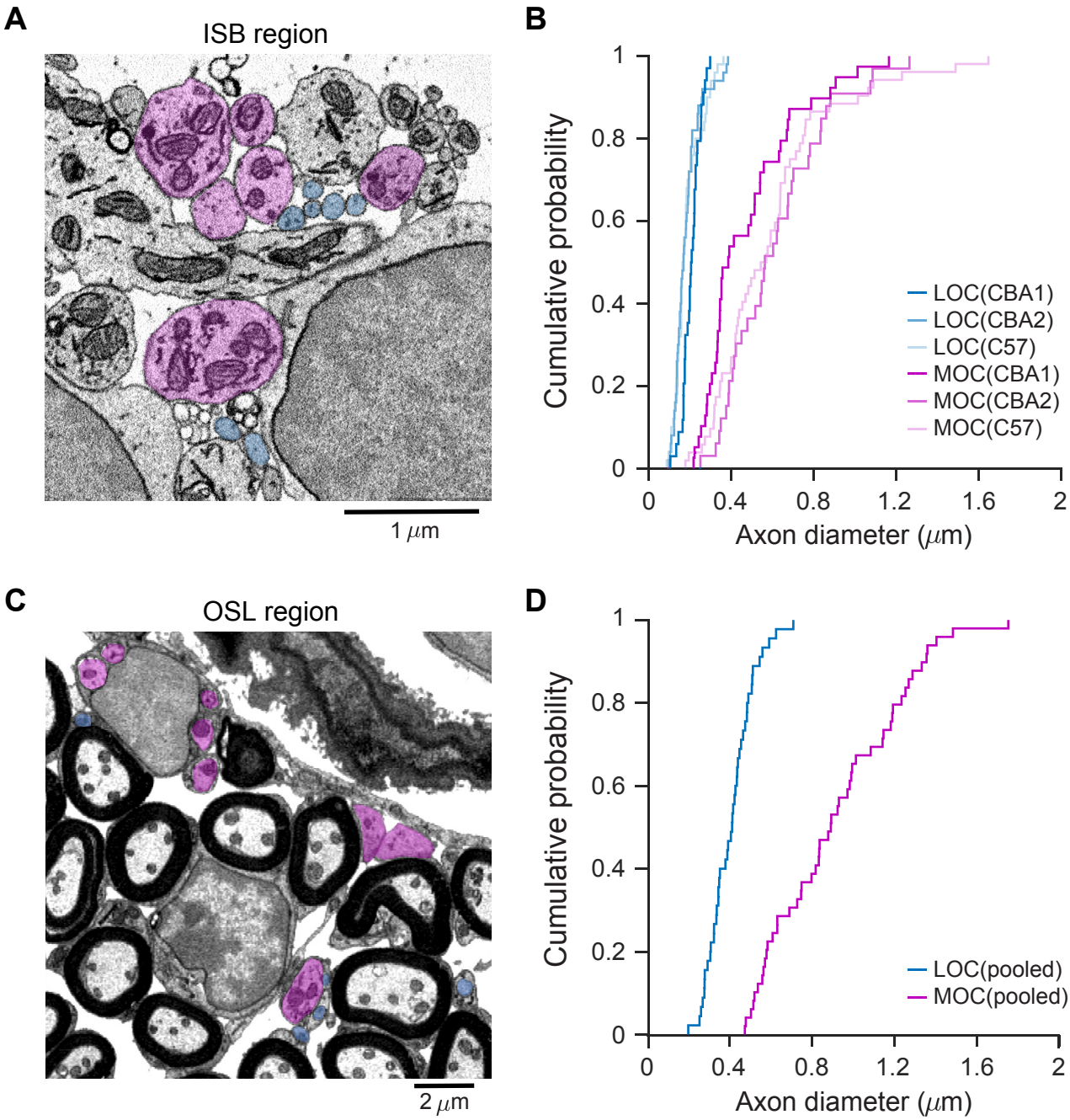

Figure S2. Distinct caliber diameter between MOC and LOC axons. Related to Figure 2 (A) Representative EM image of ISB region in which classified MOC (magenta) and LOC (blue) axons based on their innervation specificity. Scale bar 1 μm. (B) Caliber diameters were sampled from 30 non-bouton locations on randomly selected MOC and LOC axons within ISB in three datasets. Cumulative probability distributions of the axon diameters are distinct between two efferent axon classes (LOC: 208.9 ± 99.9 nm vs. MOC: 484.6 ± 284.6 nm, two-sample t-test: $p < 0.0001$). Strong systematic variability between datasets is not notable. (C) Representative EM image of osseous spiral lamina region in which classified calibers of parental MOC (magenta) and LOC (blue) axons based on their innervation specificity. Scale bar 2 μm. (D) Caliber diameters were sampled from 45 random locations of each axon class from pooled data (LOC: 402.3 ± 108.1 nm vs. MOC: 914.9 ± 315.5 nm, two-sample t-test: $p < 0.0001$).

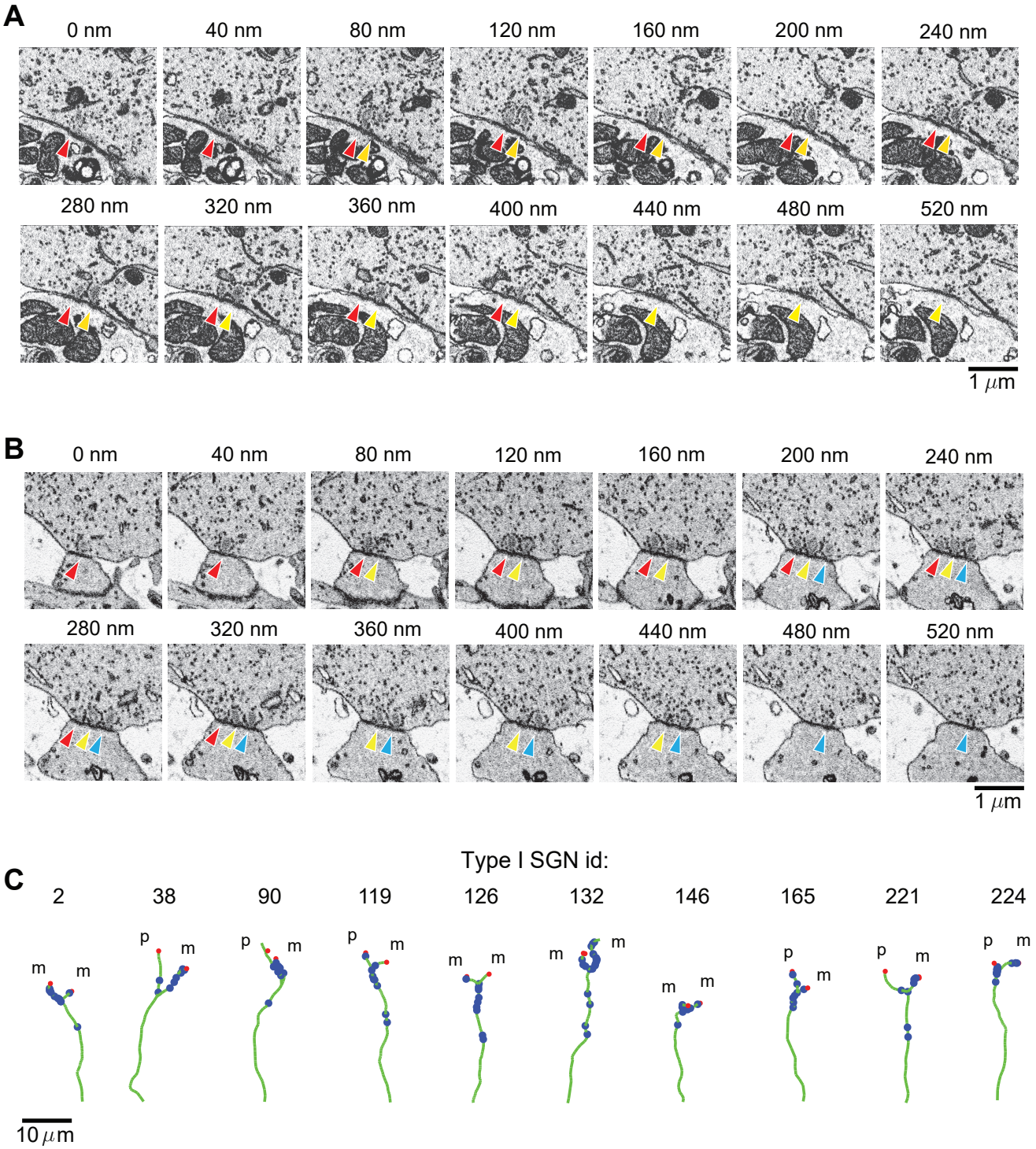

Figure S3. Multi-ribbon and branched SGN variants confirmed by SBEM. Related to Figure 3 (A and B) Consecutive sections of two example multi-ribbon structures. Distinct ribbons are pointed by arrows of different colors. Scale bar 1 µm. (C) Ten exemplary skeletons on branched SGN-dendrites. Associated ribbon and OC synapses are indicated by red and blue dots, respectively. Scale bar 10 µm.

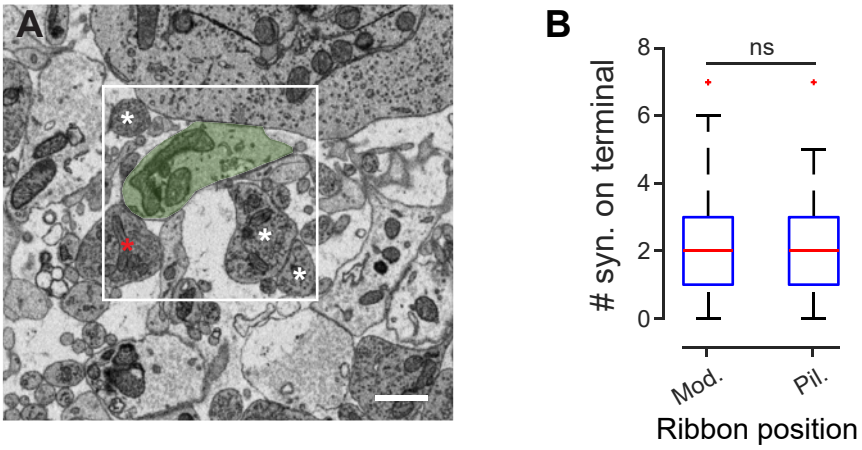

Figure S4. Similar efferent innervation of postsynaptic SGN boutons at the modiolar vs. pillar IHC faces. Related to Figure 4 (A) Exemplary image of an SGN bouton (green). Efferent synapse (indicated by physical contact of SV-filled terminal) was marked by red asterisk and those within a 4-µm-sized box (white) but without physical contact by white asterisks. Scale bar 1 µm. (B) Boxplot of efferent synapse number on SGN boutons postsynaptic to the modiolar IHC face (left) versus pillar face (right). Two-sample t-test: p = 0.0837.

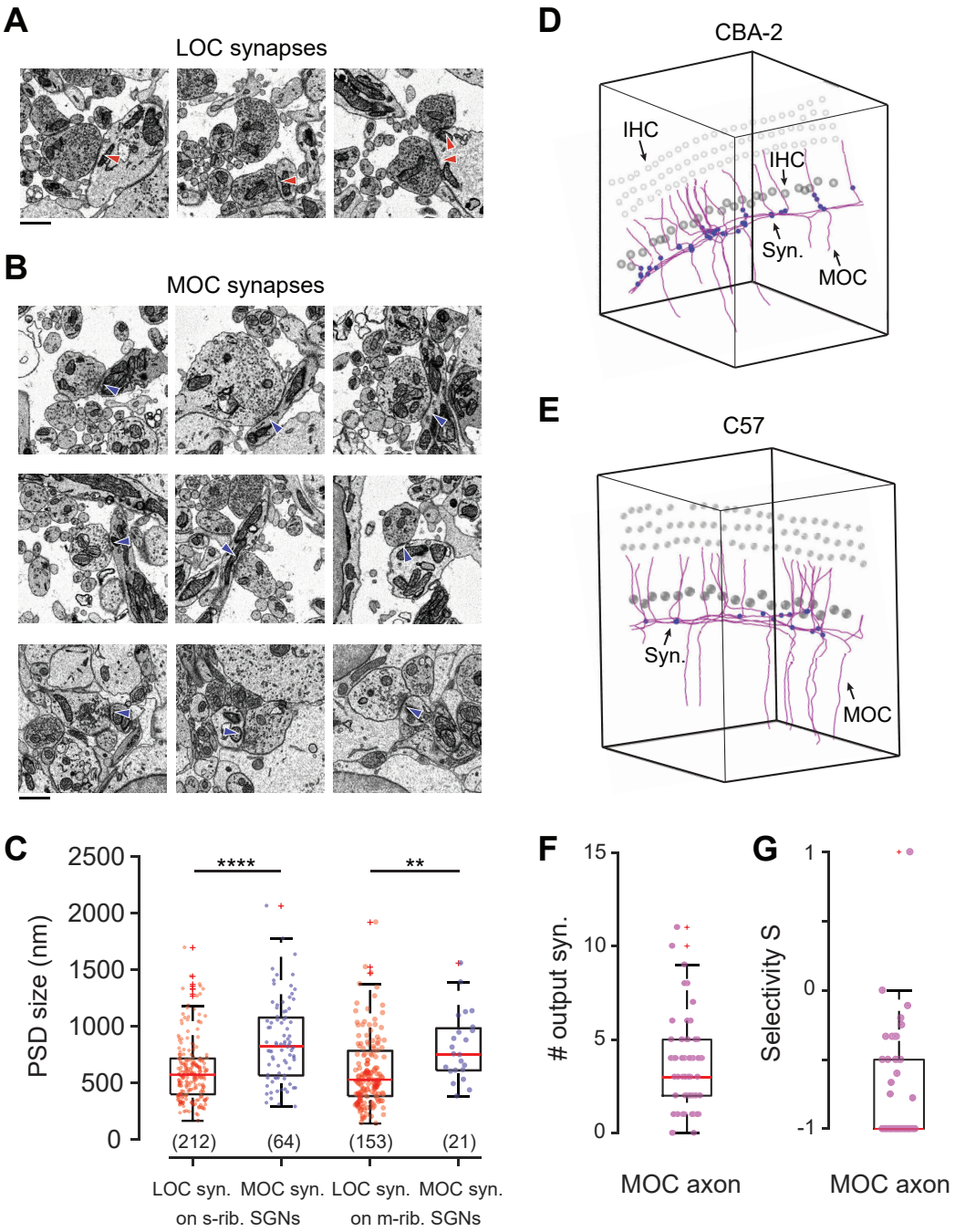

Figure S5. Distinct appearance and postsynaptic targets of MOC and LOC synapses. Related to Figure 5 (A) Representative EM images of LOC synapses (red arrows) onto SGN-dendrites. Synaptic cloud in the LOC bouton appear dense and homogenous. Scale bar 1 µm. (B) Representative EM images of MOC synapses (blue arrows) onto SGN-dendrites. In contrast to LOC synapses, MOC synapses appear to have few and sparse vesicles in the vicinity of synaptic contact. Scale bar 1 µm. (C) Comparison of post-synaptic density (PSD) size between LOC (red) and MOC synapses (blue). On both single-ribbon and multi-ribbon SGNs, LOC synapses (left: single-ribbon SGNs, 621 ± 278 nm, n = 212; middle right: multi-ribbon SGNs, 605 ± 308 nm, n = 153) had smaller PSD sizes than MOC synapses (middle left: single-ribbon SGNs, 905 ± 367 nm, n = 64; right: multi-ribbon SGNs, 802 ± 304 nm, n = 21) , whereas no significant difference were observed between LOC or MOC synapses on SGNs with different ribbon structures. Two-sample t-test: ****$p < 0.0001$ and **$p = 0.0066$. (D and E) Display of ten randomly sampled MOC fibers (magenta) with synapses (blue dots) formed on type I SGN-dendrites in the 2nd CBA animal (D) as well as C57 animal (E). (F) Boxplot showing the number of efferent synapses formed by individual MOC fibers pooled from three datasets. On average, each MOC axon formed 3.56 ± 2.40 synapses (n = 59) on SGN dendrites. (G) Innervation selectivity of MOC fibers on SGNs postsynaptic to pillar (n = 165) vs. modiolar IHC face (n = 27), selectivity index $S = (\#\ SGN_{mod.} - \#\ SGN_{pil.}) / (\#\ SGN_{mod.} + \#\ SGN_{pil.})$. Note that 43 out of 59 MOC fibers exclusively innervated pillar SGNs.

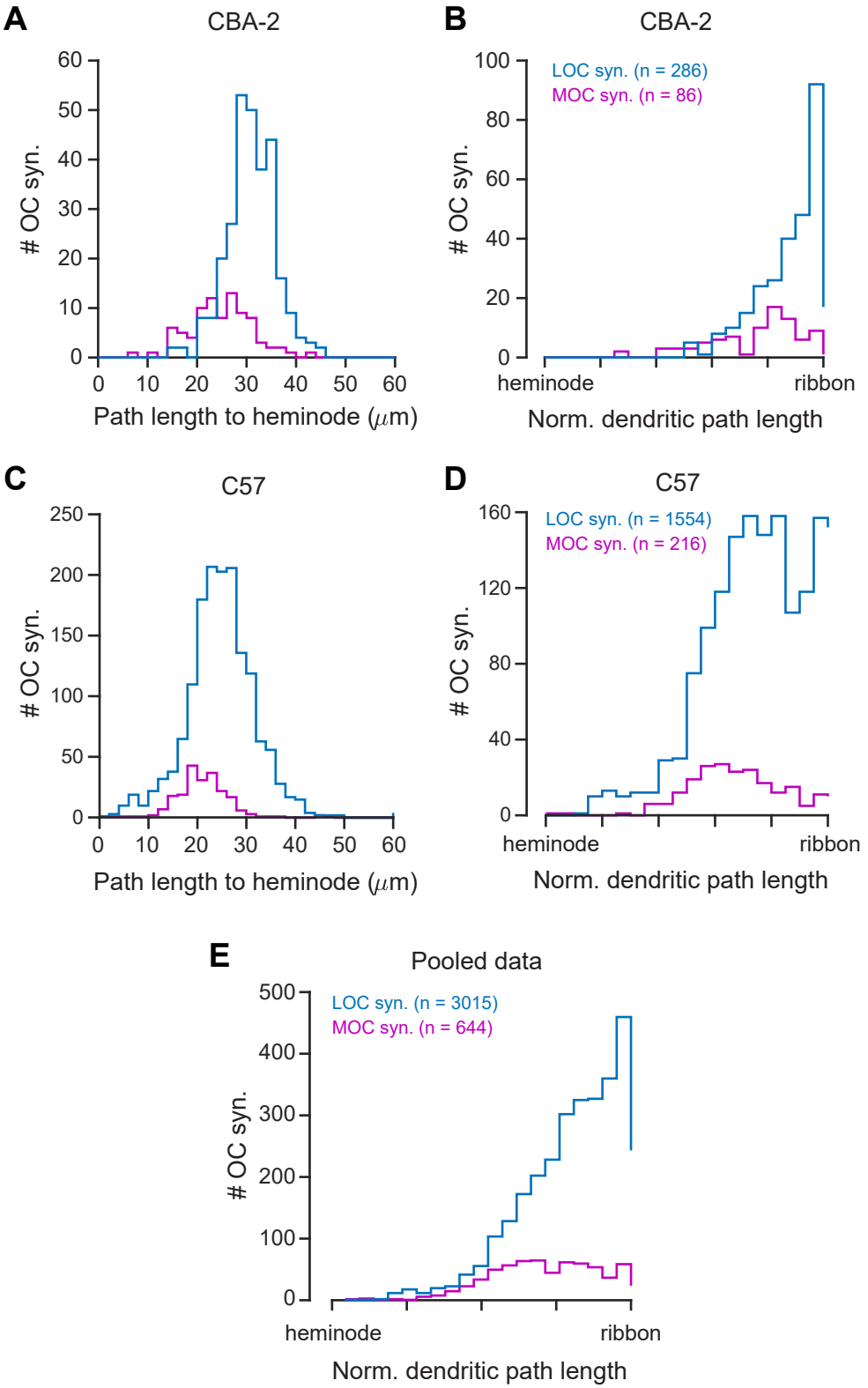

Figure S6. Same spatial arrangement of efferent innervation in the 2nd CBA animal and the C57 animal. Related to Figure 6 (A) Dendritic pathlengths in µm measured from efferent synapses to the heminode in the 2nd CBA animal. (B) Relative position of MOC synapses (magenta, n = 86) and LOC synapses (blue, n = 286) on normalized dendritic paths between ribbon AZ and heminode of SGN-dendrites. (C) Dendritic pathlengths in µm measured from efferent synapses to the heminode in the C57 animal. (D) Relative position of MOC synapses (magenta, n = 216) and LOC synapses (blue, n = 1554) on normalized dendritic paths between ribbon AZ and heminode of SGN-dendrites. (E) Relative position of MOC synapses (magenta, n = 644) and LOC synapses (blue, n = 3015) on normalized dendritic paths between ribbon AZ and heminode of SGN-dendrites of all three animals.